COMPARISON OF TRANSVERSE AND SPIN-LATTICE RELAXATION BASED ELECTRON PARAMAGNETIC RESONANCE OXYGEN IMAGES

Boris Epel and Howard J. Halpern

Center for EPR Imaging *In vivo* Physiology, University of Chicago, Department of Radiation and Cellular Oncology, MC1105, 5841 S. Maryland Avenue, Chicago, IL 60637 USA.

ABSTRACT

Recent experiments have shown that transverse relaxation (TR) T_2-based *in vivo* oxygen electron paramagnetic resonance imaging results are confounded by the effects of additional relaxation mechanisms. On the contrary, spin-lattice relaxation (SLR) T_1-based oxymetry is more precise and nearly free from those interfering mechanisms. In this article we study the differences between TR and SLR *in vivo* images by varying the spin probe concentration in an animal. We demonstrate that the dominant mechanism that differentiates TR and SLR images is the spin probe intermolecular interaction. The concentration dependence of TR observed *in vivo* is up to factor of three stronger than that in phantoms. We hypothesize that this difference is due to spin probe occupying only a small portion of the overall volume of an animal - the extracellular space. This leads to underestimation of the spin probe concentration and, hence, overestimation of concentration dependence coefficient. On the other hand, the imaging of the concentration dependence TR enhancement *in vivo* may allow investigation of the ratio of extra- and intra- cellular volumes, which is of interest for cancer biology and biomedical applications.

Index Terms— *electron paramagnetic resonance, imaging, relaxation, oxymetry, extracellular volume*

1. INTRODUCTION

To date virtually all *in vivo* time domain electron paramagnetic resonance (EPR) oxygen imaging in animal specimens has used sequences sensitive to decrease of the transverse relaxation (TR) times of the electron spin probe, T_2 [1, 2]. These measurements have been made using a tri-aryl methyl reporter molecule [3] (a trityl radical) whose unpaired electron has unusually long TR and spin-lattice (SLR) relaxation times, T_2 and T_1 respectively. The oxygen status of tissues is of crucial importance for radiotherapy and predicts the outcome of treatment [4].

In phantoms at physiologic conditions and small spin probe concentrations, the relaxation rates $R_2 = (\gamma_e T_2)^{-1}$ and $R_1 = (\gamma_e T_1)^{-1}$ are nearly equal, however, *in vivo* they show a considerable difference [5]. Here γ_e is the electron gyromagnetic ratio. Recently we demonstrated that *in vivo* T_2 images have contributions from oxygen independent relaxation mechanisms [5]. These contributions are spatially non uniform and can not be quantified from T_2 images. The *in vivo* T_1 images appear to have nearly no confounding contributions from those mechanisms. This establishes that T_1-based oxymetry is more precise and superior to T_2-based oxymetry.

In this work we study the relaxation mechanisms contributing to T_2 images. One of these mechanisms, the spin-spin intermolecular interaction has strong concentration dependence *in vitro*. In saline and at physiologic temperature, the R_2 is proportional to concentration with a proportionality coefficient of 0.83μT/mM. We speculate [5], that this dependence can explain up to a quarter of observed additional contribution to R_2 relaxation. To quantify this effect *in vivo* we performed R_1 and R_2 imaging on the same animal. R_1 images are assumed to have only oxygen dependent contributions. By varying the rate of spin probe injection the concentration in an animal can be altered and R_2 concentration dependence investigated.

2. MATERIALS AND METHODS

2.1 EPR imager and imaging protocol

A versatile pulse 250 MHz imager used to produce the images shown here has been described in detail elsewhere [6]. The transmit-receive switch of the imager was redesigned using high power components and a new low

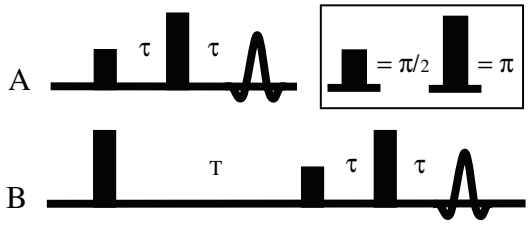

Figure 1. A. Electron spin echo (ESE) pulse sequence. B. Inversion recovery ESE (IRESE) sequence.

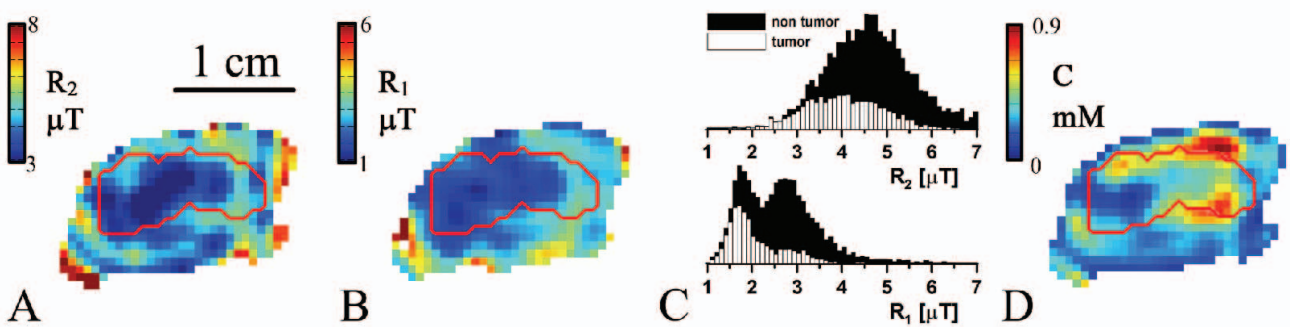

Figure 2. The selected 0.7 mm thick sagittal slices of a mouse leg bearing tumor. A. R_2 image; B. R_1 image; C. stacked histograms of R_2 and R_1 images; and D. spin probe concentration image. The tumor area determined from a registered MRI image is outlined.

noise amplifier protection scheme [7]. A pulse amplitude modulation switch was added to produce π/2- and π- pulses of equal duration (hence equal bandwidth) [8]. The imager control software SpecMan4EPR version 1.1.6 [9] was used.

For all ESE sequences the same three-dimensional FBP protocol [6] was applied: 208 projections corresponding to an 18x18 equal solid angle gradient spacing [10] were acquired; gradient strength was |**G**|=15 mT/m; object field of view was 4.24 cm. A baseline (acquisition at 1.5mT lower field) acquired every fourth trace (53 traces in all). To reduce FBP reconstruction artifacts the acquired set of projections was four-fold linearly interpolated [11] and filtered with a 3D Ram-Lak filter with a cutoff at one half of the Nyquist frequency. In the images we kept only those voxels with signal amplitude greater than 15% of the maximum amplitude at the shortest delay. Further data acquisition and processing methods are discussed in detail elsewhere [6].

2.2 T_2 EPR imaging

The transverse relaxation, T_2, is measured using two pulse electron spin echo (ESE) sequence presented in the Figure 1A. Two RF pulses of ESE sequence generate an echo, amplitude of which is dependent on the separations between pulses τ as $S(\tau) = A*\exp(-2\tau/T_2)$. An *in vivo* EPR imaging methodology based on this sequence was described by Mailer *et al.* [2].

2.3 T_1 EPR imaging

There are a number of ways to image T_1 using pulse EPR [5]. In this article we employ an inversion recovery sequence with ESE detection, IRESE (Fig. 1B). This sequence is commonly used for relaxometry [12]. The broadband π pulse inverts the spin polarization and the recovery is measured as a function of the delay T after the inversion pulse, $S(T) = A*(1 - B*\exp(-T/T_1))$. The coefficient B, $0 < B \leq 2$, accounts for incomplete inversion due to the RF field inhomogeneity in a resonator (ideally B=2, exactly).

2.4 Animal protocol

FSa tumors were grown on the right hind calves of six to eight week old C3H mice (Harlan Sprague-Dawley, Indianapolis, IN). The tumor was immobilized in the resonator by a soft, rubbery lower-body cast of vinyl polysiloxane dental impression material (GC Dental Products, Kasugai, Japan) [13] that did not affect animal physiology. At the start of imaging, 120 μL of 70 mM OX063 solution was injected into a 20 g animal (0.56 mmol/kg body weight). A continuous infusion of the same solution with the rate of ~0.80 μL/hour was maintained during the imaging. T_{1e} and T_{2e} images were sequentially taken on the same animal with no delay in between. After each pair of images an additional boost of spin probe of ~60 μL was applied and infusion rate was increased by 0.1 mL/hour to reach 0.55 mL/hour. Five to ten minutes were given to stabilize the spin probe concentration in tissues. All animal experiments were done according to the USPHS "Policy on Humane Care and Use of Laboratory Animals" and the protocols were approved by the University Of Chicago Institutional Animal Care and Use Committee. The University Of Chicago Animal Resources Center is an Association for Assessment and Accreditation of Laboratory Animal Care–approved animal care facility.

3. RESULTS

The selected slices of three dimensional relaxation rates images in a mouse are shown in Fig. 2. The relaxation rates linearly depend on oxygen. To facilitate the differences between R_2 and R_1 images, ~50% more than typical spin probe amount was injected into an animal. A tumor bearing leg has two anatomically different and easily distinguishable compartments: muscles and the tumor. Muscles are well perfused and have good supply of oxygen (higher relaxation

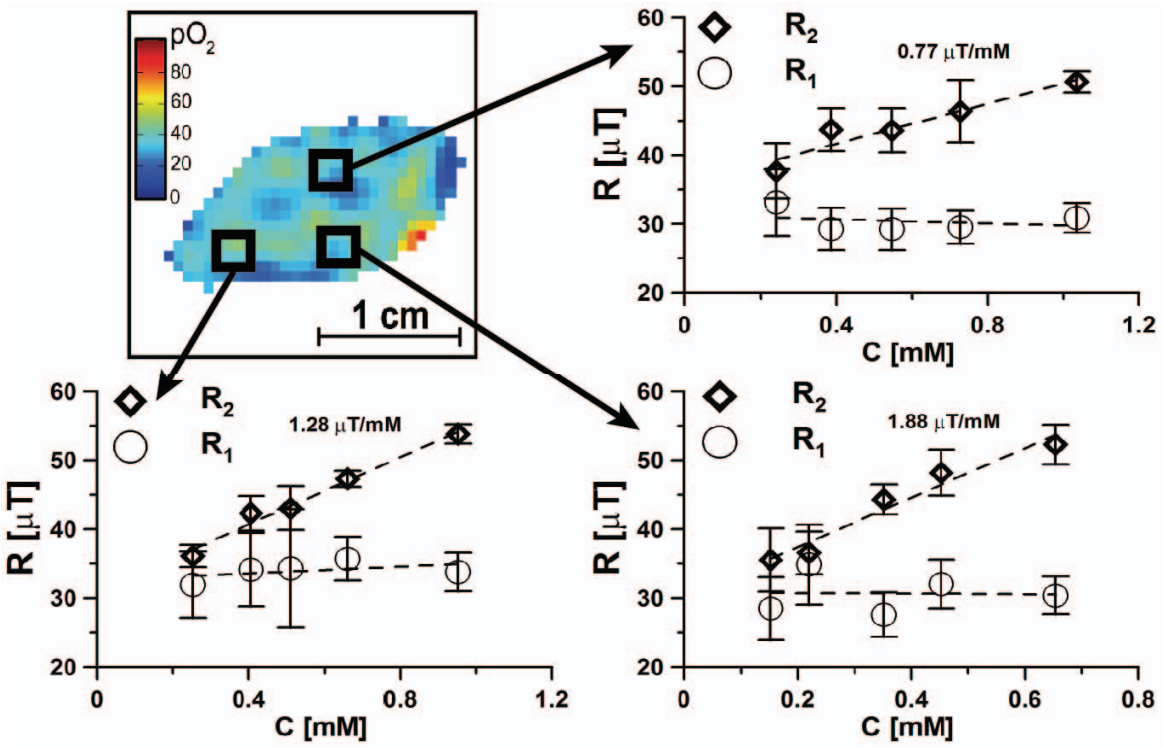

Figure 3. Relaxation rates in a mouse as a function of spin probe concentration for different experiments as spin probe is infused at different rates. Three areas of an image are visualized. The upper right plot shows the concentration dependence in the tumor while the two lower plots sample the muscle areas. The slope of R_2 concentration dependence is given in the plots.

rates) while the tumor used in this study is known to be hypoxic (lower relaxation rates). The most striking difference between R_2 and R_1 images in Figure 2 is the dramatic increase of sensitivity of R_1 to hypoxia, low oxygen, in the image manifested in the sharpening of the oxygen (relaxation rate) distribution in the tumor presented in white in the histograms (Fig. 2C). The distribution in the R_1 image exhibits two distinct modes, one of them almost entirely occupies the tumor area and other belongs to normal tissue. Another important observation is that in comparison to R_1 histogram, the histogram of R_2 images is shifted by 2-3 μT to higher values.

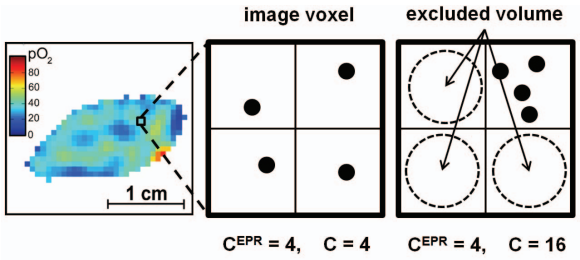

Figure 4. The effect of excluded volume on the concentration reported by an EPR image. Central panel shows uniform distribution of a spin probe in a voxel. In this case the EPR reports a correct concentration. Right panel: non-uniform distribution of spin probe. The EPR underestimates concentration by a factor of four.

Figure 3 shows the dependence of relaxation rates on the mouse spin probe concentration. The spin probe concentration was altered by selecting different rates of infusion, from low to high. A pair of R_2 and R_1 images was obtained at each infusion rate. An R_1 based oxygen image is given in the upper left panel. The concentration dependences of relaxation rates at three different spots in an image are visualized. The data are obtained by averaging rates in a 2mm cube. There is a clear trend showing an increase of R_2 with the increase of concentration, while R_1 shows no significant changes. The stable R_1 rate with concentration indicates that no substantial changes of pO_2 occurred during the experiment. The R_2 slopes of all cubes in the leg varied between 0.5 and 3 μT/mM.

4. DISCUSSION

The slope of R_2 concentration dependence measured at physiologic conditions *in vitro* is 0.83 μT/mM. The R_2 slope observed in mice varies widely and in some areas of the animal exceeds the *in vitro* slope. There is no indication in literature of the physical process that can lead to such a strong concentration dependence. We believe that other physiologic parameters that modulate R_2 such as viscosity or

salinity are not affected significantly by increased spin probe concentration.

Here we formulate the hypothesis that the increased concentration dependence of R_2 arises from the incorrect estimation of spin probe concentration in EPR *in vivo* measurements. The concentration of spin probe is a ratio of the number of spins and the volume that those spins occupy. An imaging methodology can be precisely calibrated to provide the number of spins in a voxel, a minimal volumetric image element. In a typical *in vivo* EPR image the signal for a voxel derives from a volume containing hundreds of thousands of cells. It is known that large triply charged trityl molecules can not penetrate a cell membrane and remains extracellular. Thus a substantial volume is free from spin probe. This is illustrated in the Figure 4, where a non-uniform distribution of spin probe leads to a factor of four underestimation of real concentration. This excluded volume may vary from 35-45% for blood (hematocrits) to about 65% in average in the body and up to 80% for tightly packed muscle cells [14]. Thus, the concentration reported by EPR amplitude images may be underestimated up to a factor of five, which agrees with the experiment. The quantified deviation of R_2 *vs* concentration slope from the *in vitro* value, measures the ratio between extra- and intracellular volumes.

The concentration trends for R_1 and R_2 intersect at zero concentration. Thus the only parameter that differentiates R_2 and R_1 is the spin probe concentration.

Since R_1 does not depend on concentration, the ratio between $R_2 - R_1$ and concentration can be used to estimate the slope of R_2 concentration dependence in a single experiment that does not require different infusion rates.

5. CONCLUSIONS

The difference between R_1 and R_2 images can be explained by a concentration dependence of R_2. The slope of this dependence can be understood assuming that spin probe occupies only a part of tissue volume. Variations in this slope may be due to large variations in excluded volume in tumor tissue. The difference between concentration dependence *in vivo* and *in vitro* may provide information on ratio between extra- and intracellular volumes.

6. ACKNOWLEDGEMENTS

We acknowledge our colleagues from the Center for EPR Imaging *In vivo* Physiology and NIH grants P41EB002034 and CA98575. In particular we thank Colin Mailer for useful comments and discussion.

7. REFERENCES

[1] S. Subramanian, N. Devasahayam, R. Murugesan, K. Yamada, J. Cook, A. Taube, J. B. Mitchell, J. A. B. Lohman, and M. C. Krishna, "Single-point (constant-time) imaging in radiofrequency Fourier transform electron paramagnetic resonance," *Magnetic Resonance in Medicine,* vol. 48, pp. 370-379, Aug 2002.

[2] C. Mailer, S. V. Sundramoorthy, C. A. Pelizzari, and H. J. Halpern, "Spin echo spectroscopic electron paramagnetic resonance imaging," *Magnetic Resonance in Medicine,* vol. 55, pp. 904-912, Apr 2006.

[3] J. H. Ardenkjaer-Larsen, I. Laursen, I. Leunbach, G. Ehnholm, L. G. Wistrand, J. S. Petersson, and K. Golman, "EPR and DNP properties of certain novel single electron contrast agents intended for oximetric imaging," *Journal of Magnetic Resonance,* vol. 133, pp. 1-12, Jul 1998.

[4] M. Elas, R. Bell, D. Hleihel, E. D. Barth, C. Mcfaul, C. R. Haney, J. Bielanska, K. Pustelny, K. H. Ahn, C. A. Pelizzari, M. Kocherginsky, and H. J. Halpern, "Electron paramagnetic resonance oxygen image hypoxic fraction plus radiation dose strongly correlates with tumor cure in FSA fibrosarcomas," *International Journal of Radiation Oncology Biology Physics,* vol. 71, pp. 542-549, Jun 1 2008.

[5] B. Epel, M. K. Bowman, C. Mailer, and H. J. Halpem, "T_{1e}–based Electron Paramagnetic Resonance Imaging of Oxygen *In Vivo*," *submitted,* 2010.

[6] B. Epel, S. V. Sundramoorthy, C. Mailer, and H. J. Halpern, "A versatile high speed 250-MHz pulse imager for biomedical applications," *Concepts in Magnetic Resonance Part B-Magnetic Resonance Engineering,* vol. 33B, pp. 163-176, Aug 2008.

[7] S. V. Sundramoorthy, B. Epel, C. Mailer, and H. J. Halpern, "A Passive Dual-Circulator Based Transmit/Receive Switch for Use with Reflection Resonators in Pulse Electron Paramagnetic Resonance," *Concepts in Magnetic Resonance Part B-Magnetic Resonance Engineering,* vol. 35B, pp. 133-138, Aug 2009.

[8] R. W. Quine, M. Tseytlin, S. S. Eaton, and G. R. Eaton, "A Very Fast Switched-Attenuator Circuit for Microwave and RF Applications," *Concepts in Magnetic Resonance Part B-Magnetic Resonance Engineering,* vol. 37B, pp. 39-44, Apr 2010.

[9] B. Epel, I. Gromov, S. Stoll, A. Schweiger, and D. Goldfarb, "Spectrometer manager: A versatile control software for pulse EPR spectrometers," *Concepts in Magnetic Resonance Part B-Magnetic Resonance Engineering,* vol. 26B, pp. 36-45, AUG 2005.

[10] K. H. Ahn and H. J. Halpern, "Spatially uniform sampling in 4-D EPR spectral-spatial imaging," *Journal of Magnetic Resonance,* vol. 185, pp. 152-158, Mar 2007.

[11] K. H. Ahn and H. J. Halpern, "Comparison of local and global angular interpolation applied to spectral-spatial EPR image reconstruction," *Medical Physics,* vol. 34, pp. 1047-1052, Mar 2007.

[12] A. Schweiger and G. Jeschke, *Principles of Pulse Electron Paramagnetic Resonance*: Oxford University Press, 2001.

[13] C. R. Haney, X. Fan, A. D. Parasca, G. S. Karczmar, H. J. Halpern, and C. A. Pelizzari, "Immobilization using dental material casts facilitates accurate serial and multimodality small animal imaging," *Concepts in Magnetic Resonance Part B-Magnetic Resonance Engineering,* vol. 33B, pp. 138-144, Apr 2008.

[14] W. F. Ganong, *Review of Medical Physiology*. San Mateo, CA: Appleton & Lange, 1987.